EARTH SURFACE PROCESSES AND LANDFORMS, VOL. 21, 1021–1040 (1996)

SPECTRAL ANALYSIS OF GEOMORPHIC TIME SERIES: AUTO-SPECTRUM

BRUCE J. HEGGE

D. A. Lord & Associates, PO Box 3172, LPO Broadway, Nedlands, WA 6009, Australia, and Department of Geography, University of Western Australia, Nedlands, WA 6907, Australia

GERHARD MASSELINK

Centre for Water Research, Department of Environmental Engineering, University of Western Australia, Nedlands, WA 6907, Australia

Received 28 February 1995
Accepted 25 April 1996

ABSTRACT

The collection of time series data is an essential component in the investigation of earth surface processes. Spectral analysis of these time series can provide an invaluable insight into the behaviour of geophysical processes. Spectral analysis of a single time series produces an auto-spectrum which provides a representation of the amount variance of the time series as a function of frequency. Prior to spectral analysis, the time series should be plotted to identify the presence of any trends in the mean or the variance of the series, and to identify anomalies in the data which should be corrected. To satisfy the assumption of stationarity, any trend (in either the mean or variance) should be removed from the time series. Consequently, the probability density function of the time series should be plotted and compared with the Gaussian distribution. The final stage in preparing the time series for spectral analysis is to apply a taper to reduce spectral leakage and distortion of the auto-spectrum. Following the calculation of the periodogram, spectral estimates should be combined to reduce the variability associated with the estimates and thereby ensure that the autospectrum is more representative. Finally, confidence limits should be constructed around the spectral density function so that statistically significant spectral peaks (or troughs) can be identified.

KEY WORDS spectral analysis; auto-spectrum; time series

INTRODUCTION

Earth scientists often study sequences of observations of naturally occurring processes made through time (or space). These sequences are generally referred to as 'time series' and often the process represented by the series displays some form of periodicity. In these instances an examination of the frequency components of the time series can provide a valuable insight into the behaviour of the process that generated the sequence. Spectral analysis of a single time series produces the auto-spectrum which represents the variance of the time series as a function of frequency.

Spectral methods are among the most important techniques currently employed in the study of natural systems and are widely used in geophysics, oceanography and meteorology (Båth, 1974). The rapid growth in the use of spectral techniques in a wide range of fields has led to a plethora of techniques for determining the spectra and to confusion and inconsistency in the literature (IAHR, 1989; Press *et al.*, 1989). As a result, spectral analysis is often perceived to be a technique shrouded in mystique. To add to the bewilderment, a large proportion of the literature on spectral analysis has focused on continuous infinite series. These hypothetical series provide a clear basis for theoretical analysis, but this analysis does not directly apply to the examination of natural time series, where the signal has a finite length and is typically sampled at

CCC 0197-9337/96/111021–20

discrete time steps. Furthermore, texts that do discuss the spectral analysis of finite discrete time series often present definitions that incorporate normalization of the series length and/or sample rate. This simplifies the mathematical descriptions, but confounds the practical application of spectral methods. The confusion surrounding spectral analysis has resulted in the under-use of these techniques in geomorphic investigations, although spectral analysis is not inherently complex.

The objective of this paper is to clarify the techniques of spectral analysis employed to determine the auto-spectrum and to examine the application and interpretation of these techniques when applied to natural time series. Throughout this paper a time series of nearshore water level observations will be employed to demonstrate the operation and interpretation of the techniques; however, it should be clearly noted that the techniques and methods demonstrated herein are equally applicable to any natural time series with a uniform sampling interval (e.g. river discharge, river planform, daily temperature, lake turbidity, topographic profiles). Several example time series are presented and analysed following the detailed technique description to highlight alternative means of interpreting the results of auto-spectral analysis.

The techniques covered in this paper include the determination of the periodogram, auto-spectrum, and confidence intervals of the auto-spectrum. For more detailed discussions the reader is referred to several texts, including Jenkins and Watts (1968), Rayner (1971), Båth (1974), Chatfield (1985), and Bendat and Piersol (1986).

TIME SERIES

A time series may be defined as any sequence of observations made through time, where time is the independent variable and the observed value is the dependent variable. Other series may be defined analogously in which the dependent variable is observed with respect to an ordered sequence of the independent variable (e.g. spatial series). Spectral analysis techniques are equally applicable to these series. Since time is the independent variable in the example presented in this paper, the term 'time series' will be employed throughout for convenience.

If the future state of a time series can be predicted exactly (e.g. tidal motion), then the series is considered to be *deterministic* and may be described analytically (Bendat and Piersol, 1986). However, if the future state is only partially dependent on past values, and cannot be predicted exactly (e.g. nearshore surface elevation), then the time series is *stochastic*. The analysis of these stochastic time series must be treated in terms of probability statements and statistical averages (Bendat and Piersol, 1986). Time series may be further divided into either *continuous* or *discrete*. A continuous time series has observations of the series at every point in time, whereas a discrete series consists of observations made at specific times. The time between observations in a discrete series may be either equal (uniform sampling) or unequal (non-uniform sampling). Finally, a time series may be either *stationary* or *non-stationary*. A stationary time series is one that is in statistical equilibrium, in the sense that the descriptive statistics of the series do not change with time (Jenkins and Watts, 1968). Hence, a stationary time series has no trend in either the mean or the variance. In natural systems, stationarity is often simply a matter of time scale; a time series may be stationary over a short time-span, but not over an extended period.

A time series may be represented in three distinct domains, each of which has its own independent variable, analysis techniques and analysis objectives. The *time series* is an expression of the observed values in the time domain in which time is the independent variable. The *probability density function* represents the series in the amplitude domain in which amplitude is the independent variable. The *auto-spectrum* is a representation of the series in the frequency domain where frequency is the independent variable.

A range of statistical methods is available to examine the frequency components of a time series, including the semi-variogram (Davis, 1986), autocorrelation function (Davis, 1986), harmonic analysis (Godin, 1972), higher-order non-Fourier techniques (Kay and Marple, 1981), and spectral analysis (Bendat and Piersol, 1986). The semi-variogram and autocorrelation functions have been used in several geomorphic investigations including studies of stream and gully profiles (Richards, 1976; Anderson and Richards, 1979), river meanders (Speight, 1965; Thakur and Scheidegger, 1970; Ferguson, 1975, 1976), topographic variability (Mulla, 1988) and sandy bedforms (Robert and Richards, 1988). The semi-variogram and autocorrelation

functions do not require such stringent stationarity assumptions as does spectral analysis and can be used on shorter time series. For time series which represent a truly periodic phenomena, such as a tidal record, harmonic analysis may be used to decompose the series into its constituent parts (cf. Godin, 1972). Higher-order non-Fourier techniques include the maximum entropy method, Pisarenko harmonic decomposition and Walsh functions (Båth, 1974; Kay and Marple, 1981; Beauchamp, 1984). The interest in these non-Fourier techniques is primarily due to the apparent high-resolution performance that can be achieved for series of limited length (Marple, 1987). However, Kay and Marple (1981) review a number of techniques and note that the degree of improvement of these non-Fourier techniques, compared with Fourier techniques, is largely dependent on the signal-to-noise ratio. Where this is low, as for most natural time series, the Fourier and non-Fourier methods provide comparable results.

Spectral analysis has been widely employed in geomorphic studies to examine the frequency constituents of time series including studies of oscillatory currents (Hardisty, 1993), swash motion (Guza and Thornton, 1982; Holman and Sallenger, 1985), ocean waves (Kinsman, 1984), river meanders (Ferguson, 1975), annual temperature variations (Craddock, 1956) and topographic variability (Young and Pielke, 1983; Young *et al.*, 1984; Mulla, 1988). Spectral analysis has several advantages in that it enables the fine-scale resolution of a range of frequency components and may be extended to examine (1) relationships between series, and (2) non-linear relationships both between frequency components and between series. Modern-day spectral analysis is based on the Fourier transform which is computationally efficient, robust and yields reliable results for a large class of time series; consequently this technique has become one of the most popular methods for the examination of frequency components in a series and is therefore the focus of the present paper.

THE FOURIER TRANSFORM

Continuous Fourier transform

A physical process can be described in the time domain by the value of a quantity as a function of time (e.g. $x(t)$ for $-\infty < t < \infty$) or in the frequency domain where the process can be described by its amplitude and phase as a function of frequency (e.g. $X(f)$ for, $-\infty < f < \infty$, where $X(f)$ is generally a complex number) (Press *et al.*, 1989). Thus, $x(t)$ and $X(f)$ are two different representations of the same function and are directly related via the Fourier transform:

$$X(f) = \int_{-\infty}^{\infty} x(t) e^{-2\pi i f t} dt \tag{1}$$

and the inverse Fourier transform:

$$x(t) = \int_{-\infty}^{\infty} X(f) e^{2\pi i f t} df \tag{2}$$

The Fourier transform pair allow a function to be expressed in the frequency domain (Equation 1) or in the time domain (Equation 2). These two transforms constitute an exact complement; there are no error terms and no information is lost via this transformation. The Fourier transform (Equation 1) represents the time series $x(t)$ in terms of the distribution of its variance at different frequencies. The transform pair are normalized so that the total variance is the same whether calculated in the time or the frequency domain. This is formalized by Parseval's theorem, which states (for a time series with a mean of zero):

$$\text{Total variance} \equiv \int_{-\infty}^{\infty} |x(t)|^2 dt = \int_{-\infty}^{\infty} |X(f)|^2 df \tag{3}$$

Equations 1, 2 and 3 are only applicable to continuously sampled, infinite time series. However, in practice, it is generally only possible to analyse a discretely sampled, finite time series. This apparently minor modification has profound implications (Press *et al.*, 1989) that necessitate the formulation of the discrete Fourier transform (DFT).

Discrete Fourier transform

The Fourier transform of a finite time series $x(n)$ of length N, sampled at a uniform sampling frequency, may be expressed as (cf. Equation 1):

$$X(k) = \sum_{n=0}^{N-1} x(n) e^{-2\pi i k n/N} \qquad k = 0, 1, \ldots, N-1 \tag{4}$$

A geometric insight into the discrete Fourier transform may be gained by expressing Equation 4 in complex polar notation:

$$X(k) = \sum_{n=0}^{N-1} x(n) \left(\cos \frac{2\pi k n}{N} - i \sin \frac{2\pi k n}{N} \right) \qquad k = 0, 1, \ldots, N-1 \tag{5}$$

It follows that the discrete Fourier series $X(k)$ is a complex series of the same length (N) as the original time series $x(n)$ and is composed of a real cosine part and an imaginary sine element.

Equation 5 may be redefined in terms of the Fourier cosine $a(k)$ and sine $b(k)$ coefficients:

$$X(k) = a(k) - ib(k) \qquad k - 0, 1, \ldots N-1 \tag{6}$$

where

$$a(k) = \sum_{n=0}^{N-1} x(n) \cos \frac{2\pi k n}{N} \tag{7a}$$

$$b(k) = \sum_{n=0}^{N-1} x(n) \sin \frac{2\pi k n}{N} \tag{7b}$$

The frequency of the kth Fourier coefficient is determined by the sampling frequency f_s, and the length of the series N:

$$f_k = k f_s / N \tag{8}$$

It follows from Equation 8 that the frequency resolution or binwidth (i.e. the interval between adjacent frequency bins) is equal to f_s/N. In summary, the Fourier transform allows a time series to be represented by a series of cosines and sines whose frequencies are multiples of f_s/N.

The Fourier coefficients of an eight-point example record are shown in Table I. The first point of the discrete Fourier series ($X(0)$) is known as the DC value and has a frequency $f_0 = 0$. This point is a real number and is equal to the sum of the time series. If a time series is detrended prior to calculating the discrete Fourier transform, then $X(0)$ will be zero. The second point of the discrete Fourier series $X(1)$ has a frequency equal

Table I. Discrete Fourier transform of a series of eight points ($N = 8$; $f_s = 4$ Hz)

Time index n	Time series observation $x(n)$ (m)	Fourier transform index k	Fourier series $X(k)$			Fourier frequency f_k (Hz)	Periodogram (double sided) $P(k)$ ($m^2 Hz^{-1}$)	Phase (double sided) $\theta(k)$ (radians)
0	0·5833	0	0·0000			0·0	0·0000	0·0000
1	−1·0476	1	2·1096	−	i1·2646	0·5 (= f_f)	0·1890	−0·5400
2	0·3214	2	−2·4762	+	i5·4762	1·0	1·1288	−1·1461
3	2·6905	3	4·9380	−	i0·2170	1·5	0·7635	−0·0439
4	−2·9405	4	−4·4762			2·0 (= f_c)	0·6261	0·0000
5	−0·5714	5	4·9380	+	i0·2170	2·5	0·7635	0·0439
6	−0·2024	6	−2·4762	−	i5·4762	3·0	1·1288	1·1461
7	1·1667	7	2·1096	+	I1·2646	3·5	0·1890	0·5400

to the fundamental frequency $f_1 = f_s/N \equiv f_f$. The fundamental frequency is the lowest frequency which can be determined from the time series using Fourier techniques. The middle point of the discrete Fourier series $X(N/2)$ is a real number and represents the variance of the highest frequency that may be resolved using the discrete Fourier transform. This frequency is known as the folding or Nyquist frequency (f_c) and is directly determined by the sampling frequency:

$$f_c \equiv f_{N/2} = f_s/2 \tag{9}$$

Natural time series generally consist of real-valued data and in these instances the Fourier coefficients beyond the Nyquist frequency represent negative frequencies. These negative frequencies have no physical meaning and do not provide additional information since they are complex conjugates of the first half of the Fourier series (cf. Table I).

An unfortunate, but unavoidable, result of calculating the discrete Fourier transform is that the variance of oscillations with frequencies higher than the Nyquist frequency are spuriously included in the frequency range from f_0 to f_c. This phenomenon is termed 'aliasing' and is encapsulated in Parseval's theorem (Equation 3), which states that all the variance in the time series is contained within the Fourier series and distributed between frequencies f_0 and f_c. Two steps can be taken to minimize the effect of aliasing. First, one should ensure that the sampling frequency is chosen such that oscillations at frequencies greater than half the sampling frequency are minimized. Second, the signal can be filtered to eliminate high frequency components prior to digitization. An indication of the degree of aliasing can be obtained by examining the magnitude of the spectral density at frequencies approaching f_c; if the spectral density at these frequencies approaches zero, then aliasing should be minimized.

OBTAINING THE FOURIER COEFFICIENTS

The cosine ($a(k)$) and ($b(k)$) coefficients of Equation 6 provide the foundation of Fourier-based spectral analysis. However, the direct calculation of these coefficients using Equations 7a and 7b is particularly inefficient and several alternative methods have been developed. For some time, direct estimation of the spectrum was conducted through the use of special purpose analogue devices (e.g. harmonic analysers, filter banks, wave analysers); however, these physical techniques did not gain widespread use (Bingham *et al.*, 1967). It was not until electronic computers came into general use that spectral analysis of geophysical phenomena really began (Båth, 1974). The wide applicability and numerical accuracy of digital methods has clearly established this technique over analogue methods (Beauchamp and Yuen, 1979).

The Fourier coefficients of a time series may be obtained indirectly via the autocorrelation function, commonly termed the Blackman–Tukey method (Blackman and Tukey, 1958). This approach exploits the fact that the autocorrelation function and the spectral density function form a Fourier pair. The Blackman–Tukey method remained the most popular method for determining the Fourier series until the popularization of the fast Fourier transform (FFT) by Cooley and Tukey (1965).

The FFT algorithm is a non-obvious computational procedure that determines the Fourier coefficients directly from the time series by exploiting the binary notation employed in digital computers. This algorithm works most efficiently when the length of the time series is an integer power of 2 (i.e. $N = 2^h$, where h is a positive integer). The FFT procedure is significantly faster than the indirect autocorrelation method and remains the workhorse of modern spectral analysis (MATLAB, 1990).

Spectral analysis of non-stationary data, using the traditional techniques, is not appropriate, hence it is necessary to remove any trend in the series prior to analysis. A trend in the mean is traditionally removed by fitting a polynomial curve to the data—usually linear, but occasionally quadratic—and subtracting this curve from the data. There are several alternative methods of trend removal, including filtering, differencing and fitting piecewise polynomials (Chatfield, 1985). If trends in the mean are not removed prior to analysis, the resulting spectrum will be dominated by energy at the lower end of the frequency scale. If a trend is apparent in the variance of the time series it may be possible to split the series into several parts and analyse these independently. If this is not possible, Båth (1974) provides a discussion of spectral analysis techniques that are directly applicable to time series in which the variance changes over time.

NEARSHORE DATA

The example time series presented here was obtained from a wave recorder located in the nearshore zone of Nine Mile Beach, Central Queensland (Australia). The data were collected at high tide as part of a larger study on the morphodynamics of macrotidal beaches (Masselink, 1995; Masselink and Hegge, 1996). The wave recorder was located in the mid-surf zone (mean water depth 1·8 m) and measured predominantly breaking and broken swell waves with heights up to 1·5 m (Figure 1).

The water surface elevation was sampled at a frequency of 4 Hz ($f_s = 4$) for a period of 34 min ($n = 8192$). This sample provided a sufficient record length to examine wave periods up to 1 min and was sampled at a sufficiently high frequency to minimize the spurious effects of aliasing. The data were obtained under relatively still tide conditions, and no trend was apparent in the water level or wave heights. However, as a precaution, the time series was linearly detrended prior to further analysis.

The probability density function of the water surface elevation is positively skewed and differs from a Gaussian distribution (Figure 2). The positive skewness of the probability density function is typical of surf zone waves which are characterized by sharp peaks and flat troughs (Figure 1). Many geomorphic processes produce time series that do not have normally distributed probability density functions. Auto-spectral analysis of these non-Gaussian time series is still appropriate; however, care should be taken in the interpretation of confidence intervals.

CALCULATING THE AUTO-SPECTRUM

The periodogram

Following the computation of the Fourier coefficients, the calculation of the periodogram is the first step in the determination of the auto-spectrum. The one-sided periodogram may be defined as:

$$P(k) = \frac{|X(k)|^2}{f_s N} \qquad \text{for } k = 0, \frac{N}{2} \tag{10a}$$

$$P(k) = \frac{2|X(k)|^2}{f_s N} \qquad \text{for } k = 1, \ldots \frac{N}{2} - 1 \tag{10a}$$

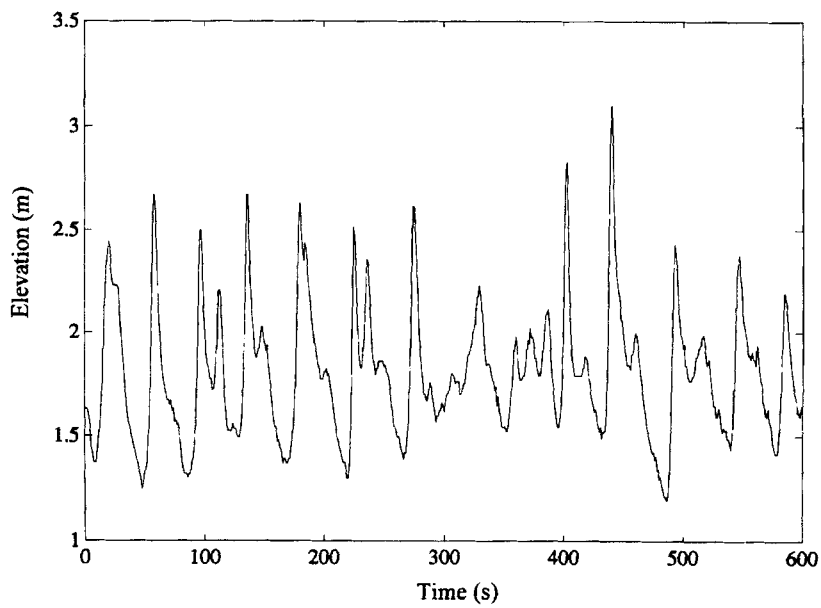

Figure 1. Section of the time series of nearshore surface elevation collected from Nine Mile Beach, sampled at 4 Hz

or equivalently:

$$P(k) = \frac{a(k)^2 + b(k)^2}{f_s N} \qquad \text{for } k = 0, \frac{N}{2} \tag{10b}$$

$$P(k) = \frac{2(a(k)^2 + b(k)^2)}{f_s N} \qquad \text{for } k = 1, \ldots, \frac{N}{2} - 1 \tag{10b}$$

It should be noted that only the first half of the Fourier series is used in the calculation of the periodogram, since the Fourier coefficients beyond the Nyquist frequency are complex conjugates (i.e. $a + ib$ is the complex conjugate of $a - ib$). To compensate for this, the Fourier coefficients, excepting $P(0)$ and $P(N/2)$, are doubled. The one-sided periodogram is normalized such that the sum of $P(k)$ is proportional to the variance of the time series (Parseval's theorem; Equation 3):

$$\text{Variance} \equiv \frac{1}{N}\sum_{n=0}^{N-1} x(n)^2 = \frac{f_s}{N}\sum_{k=0}^{N/2} P(k) \tag{11}$$

If the original time series was sampled in units of metres and the sampling period was measured in units of seconds, then the resulting periodogram $P(k)$ has units of metres squared seconds (m^2 s) or, equivalently, metres squared per Hertz (m^2 Hz^{-1}). $P(k)$ has been variously termed variance-spectral density, power-spectral density and energy-spectral density. For ocean waves the term 'variance-spectral density' or simply 'spectral density' is recommended by the International Association for Hydraulic Research (IAHR, 1989) and will be used throughout this paper.

The periodogram may be presented visually by plotting frequency f_k (Equation 8) on the ordinate and spectral density $P(k)$ (Equation 10) on the abscissa. Since the spectral density is determined as an average over a small frequency band, centred at the discrete Fourier frequencies (f_k), it is appropriate to present the periodogram as a histogram (Båth, 1974). However, for presentation purposes the periodogram is typically presented as a line plot. The location of the peaks, and/or troughs, on the frequency axis is generally

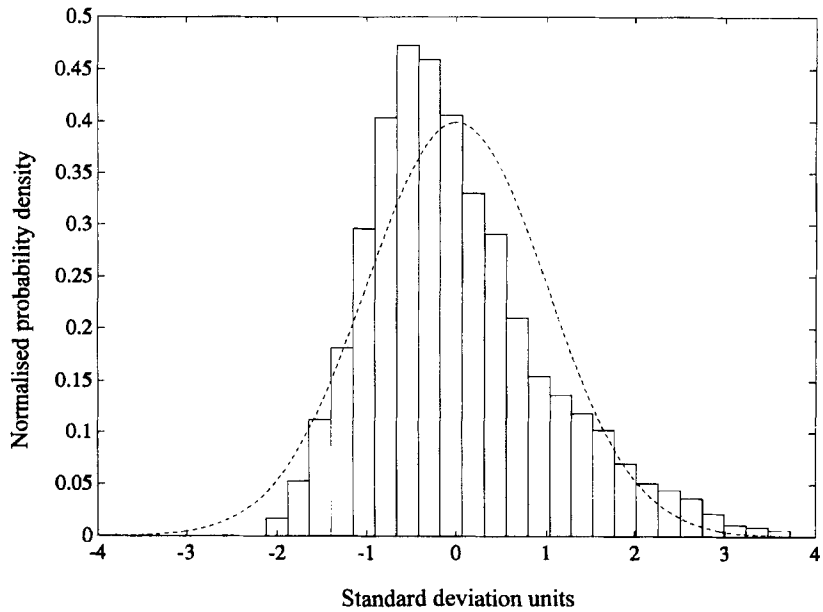

Figure 2. Standardized probability density function of the time series of nearshore surface elevation (standard deviation = 0·3543). The dotted line represents the normal distribution

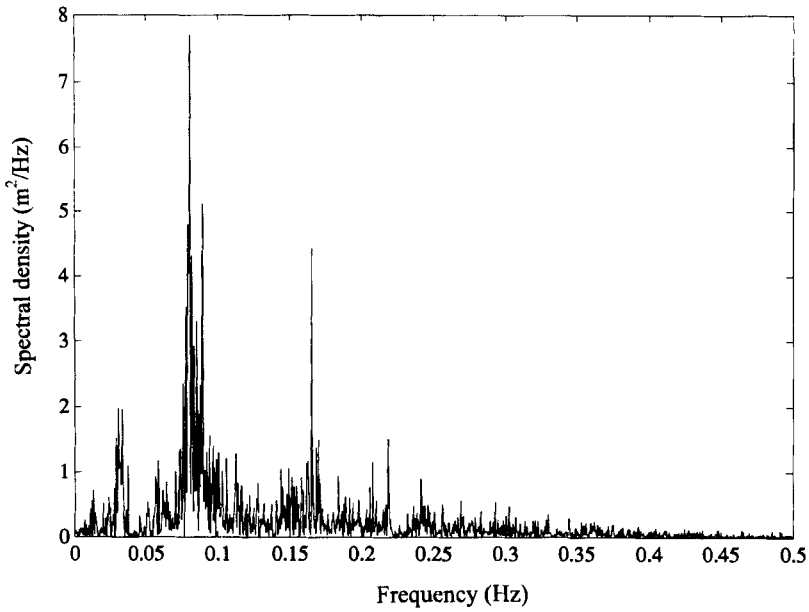

Figure 3. Periodogram of the surface elevation record ($N = 8192, f_s = 4$ Hz, $\nu = 2$ and bin width = 0·0004883 Hz). Note that only the frequencies up to 0·5 Hz are shown; frequencies from 0·5 to 2 Hz have very little spectral energy and are therefore not presented

more important than the absolute value of the spectral density associated with them (Båth, 1974). However, when determining the proportion of energy contained within certain frequency limits, the actual value of the spectral density is of importance.

The phase of each Fourier frequency $\theta(k)$, with respect to the beginning of the series, may be expressed as:

$$\theta(k) = \arctan \frac{b(k)}{a(k)} \qquad k = 0, \ldots \frac{N}{2} \tag{12}$$

The phase function $\theta(k)$ has units of radians; however, the phase function of a single time series is formally considered to be entirely random and is therefore of no statistical importance.

The periodogram of the Nine Mile Beach wave record shows that there is minimal energy at frequencies higher than 0·4 Hz; this confirms that the sample frequency chosen was sufficiently high to minimize the effects of aliasing (Figure 3). Three peaks are apparent at the low frequency end of the spectrum and represent infragravity waves (0·03 Hz), swell waves (0·08 Hz) and the first harmonic of the swell waves (0·16 Hz, twice the frequency of the primary swell waves) (cf. Carter, 1988). The combination of the primary swell waves and the first harmonic largely account for the peaked nature of the surf zone wave record.

Tapering to reduce spectral leakage

As noted above, any natural time series available for analysis must be of a finite length. The discontinuities presented by the two end points of the series introduce distortion into the calculated spectral density function. This distortion is referred to as 'leakage', whereby the value of a spectral estimate is reduced through leakage of spectral energy to neighbouring frequency bins. Leakage is a particular problem for narrow-banded signals and/or short time series.

Leakage may be minimized by eliminating the discontinuities at the extremes of the time series by causing the end points to move smoothly towards zero (Press *et al.*, 1989). This is termed 'tapering' and there are many tapering functions available, the most common of which are rectangular (box-car), triangular, sine, cosine, Hann and Hamming. The tapering functions define a series of weights that are applied to the time series prior to determining the Fourier coefficients (Figure 4). The use of no taper is equivalent to using a

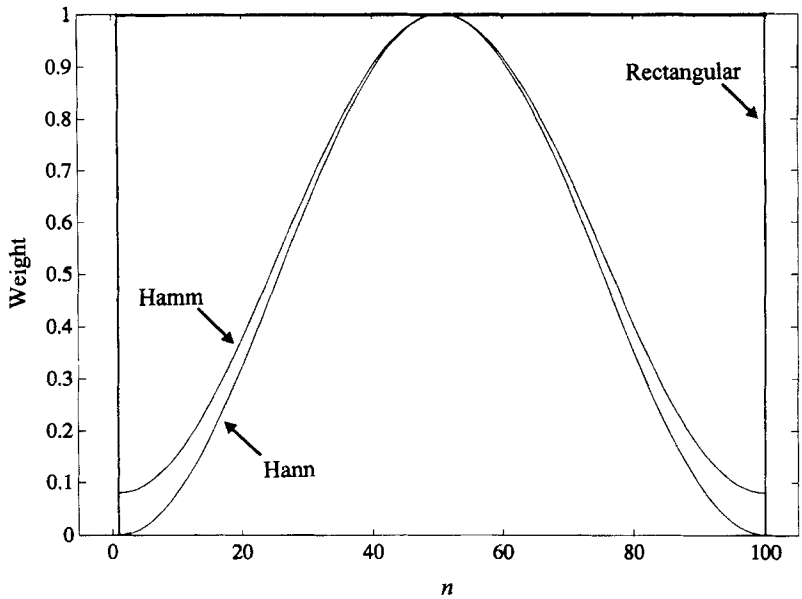

Figure 4. Rectangular, Hann and Hamming tapering functions

rectangular taper. The application of a taper inevitably reduces the frequency resolution of the periodogram; however, this loss is generally an acceptable penalty to pay for the minimization of leakage (Bendat and Piersol, 1986).

The Hann taper has gained widespread use in geophysics (Båth, 1974) and is defined as:

$$w(n) = 0{\cdot}5\left(1 - \cos\frac{2\pi n}{N-1}\right) \qquad n = 1, 2, \ldots, N \tag{13}$$

Taper functions are applied directly to the time series by multiplying the time series $x(n)$ by the taper $w(n)$. Consequently the periodogram (Equation 10) is determined from the tapered time series. Since tapering essentially discards relevant information at the beginning and end points of a time series, the total variance of the series is decreased (Bendat and Piersol, 1986). To correct for this loss of variance, and hence satisfy Parseval's theorem (Equation 11), it is necessary to apply a correction factor to each of the spectral density estimates. The correction factor C for any taper is inversely proportional to the variance of the taper:

$$C = \frac{N}{\sum_{n=1}^{N} w(n)^2} \tag{14}$$

For the Hann taper (Equation 3) the correction factor is equal to 8/3.

The application of a taper prior to the calculation of the periodogram considerably improves the distinction of the peaks, in particular the infragravity peak (Figure 5). However, in this example it appears that the Hann or Hamming tapers yield comparable results.

Variance of the spectral estimates

The periodogram provides an alternative representation of a time series. Since any natural time series describes a stochastic process that fluctuates unpredictably, it follows that the spectral estimates of the periodogram can vary unpredictably and are therefore statistically unreliable. The number of degrees of freedom (ν) associated with the periodogram provides an indication of the reliability of the spectral estimates. The reliability of the periodogram $P(k)$ is very low—$P(0)$ and $P(f_c)$ have one degree of freedom, whereas all other spectral estimates of the periodogram have two degrees of freedom ($\nu = 2$) (Beauchamp and Yuen,

1979) (Equation 10). A more reliable description of the stochastic process represented by the time series may be gained by combining spectral estimates. Two methods are generally used to accomplish this, bin-averaging and segment-averaging (Welch method).

(1) *Bin-averaging*. Since the time series represents a sample from a stochastic process it follows that adjacent frequency bins of the periodogram are independent. Thus, perhaps the simplest way of reducing the variability of the spectral estimates is by averaging estimates over adjacent frequency bins to obtain a spectral estimate $S(j)$ for the mid-frequency bin. In this instance, the number of degrees of freedom

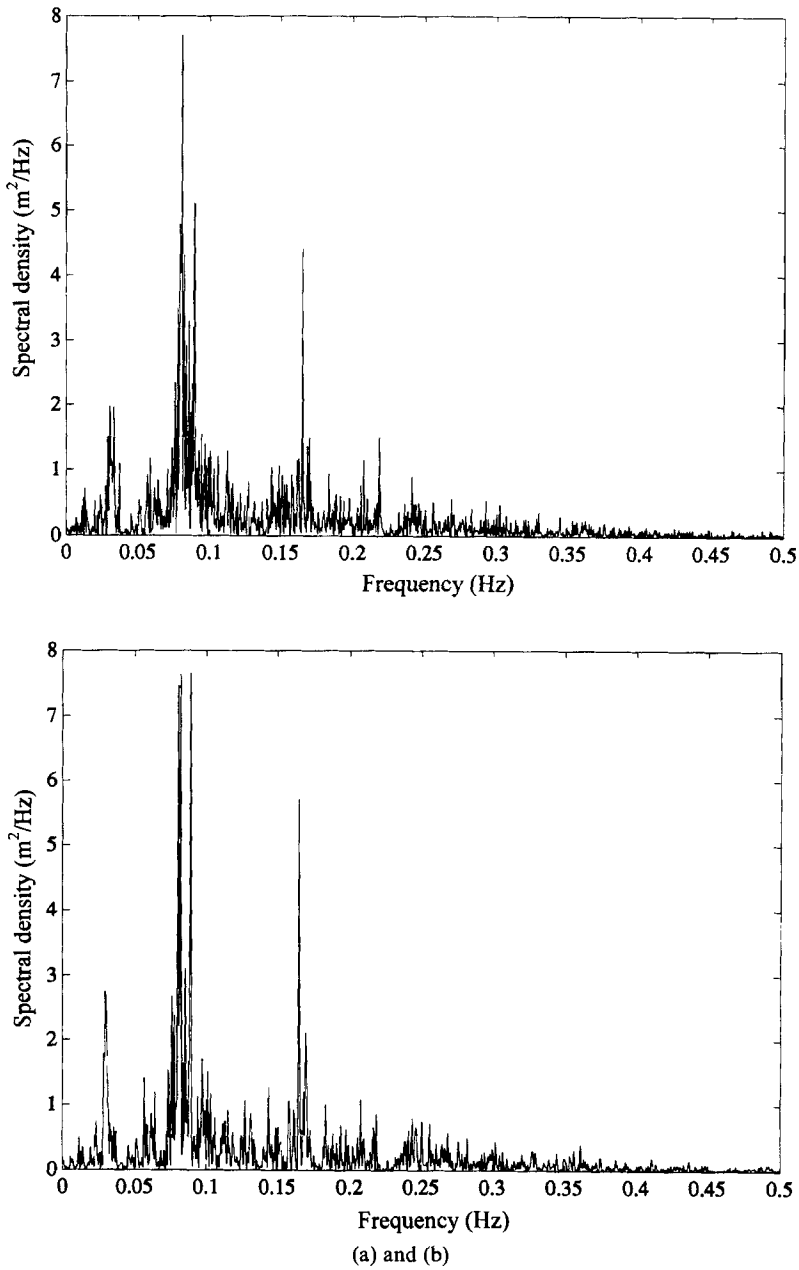

(a) and (b)

Figure 5. Periodograms of the water surface elevation record obtained using (a) a boxcar taper; (b) a Hann taper; and (c) a Hamming taper function. For all periodograms, $N = 8192$, $f_s = 4$ Hz, $\nu = 2$ and bin width = 0·0004883 Hz

(ν) is equal to twice the number of adjacent frequency bins averaged. The bin-averaging method is straightforward, but can be computationally inefficient for long time series (Press *et al.*, 1989).

(2) *Segment-averaging*. Since the time series is assumed to be both stochastic and stationary, it follows that periodograms of adjacent time segments are independent. Thus, an alternative approach to reducing the variance of the spectral estimates is to partition the time series into m smaller segments of equal length and determine a periodogram for each segment. Subsequently, the m periodograms are averaged at each frequency bin to obtain the spectral estimates $S(j)$. In this instance the number of degrees of freedom (ν) is equal to twice the number of segments. To obtain a near-maximum reduction in the variance of the spectral estimates from a fixed number of points, a reasonable procedure is to overlap the segments by half their length (Welch, 1967). In this instance, the number of degrees of freedom can be roughly approximated as twice the total number of segments. The actual degrees of freedom, when using 50 per cent overlapping segments, is slightly less than this value since the individual segments are not independent. The calculation of the exact degrees of freedom is not straightforward and involves a consideration of the degree of overlap and the taper function used. The segment-averaging method is particularly efficient for long time series. However, as each individual segment is detrended prior to computing the Fourier coefficients, a proportion of the low-frequency energy will be lost.

The spectrum of the wave record from Nine Mile Beach was calculated using three different techniques: bin-averaging, and segment-averaging with and without 50 per cent overlap (Figure 6). The most apparent difference between the periodogram and these spectra is the substantial loss of resolution which helps to facilitate the interpretation of the spectra. The three energy bands identified in the periodogram are more distinct in each of the three spectra. As expected, the three techniques do not produce markedly different spectra, though it is apparent that the bin-averaging technique produced a spectrum with more accentuated peaks in the infragravity and first harmonic frequency bands.

Confidence limits about the spectral estimates are determined from the number of degrees of freedom. For a Gaussian-distributed time series the confidence limits are related to the degrees of freedom through the chi-squared distribution (Bendat and Piersol, 1986):

$$S(j)\frac{\nu}{\chi^2_{\nu,1-\alpha/2}} \geqslant S(j) \geqslant S(j)\frac{\nu}{\chi^2_{\nu,\alpha/2}} \tag{15}$$

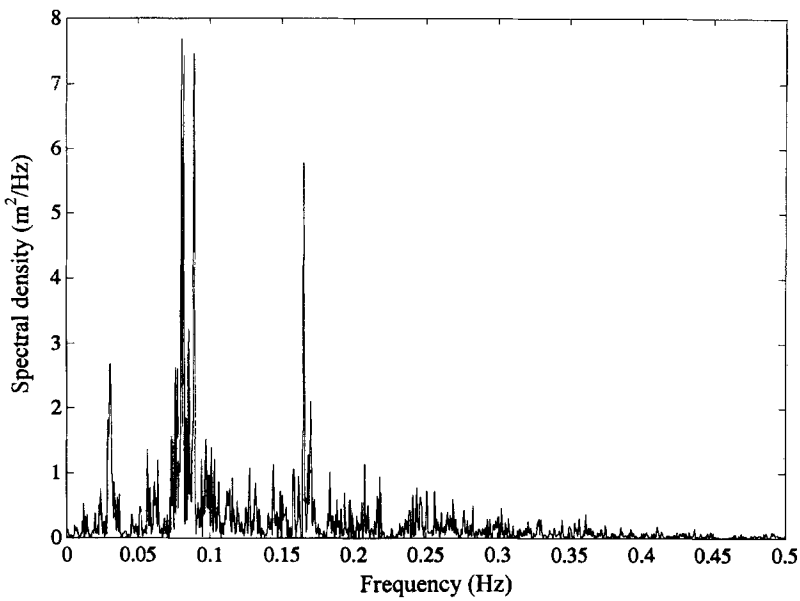

(c)

A percentage significance level of 95 per cent (i.e. $\alpha = 0{\cdot}05$) is commonly applied in geophysics. It is commonly assumed that the probability density function of the time series is Gaussian. However, for time series that are distinctly non-Gaussian, care must be taken in interpreting the confidence limits.

Both the bin-averaging and the segment-averaging methods reduce the variance associated with the spectral estimates by a factor of m. Unfortunately, this is offset by a loss of frequency resolution since the bin-width of the density spectrum becomes $f_s m/N$ and is increased from that of the periodogram by a

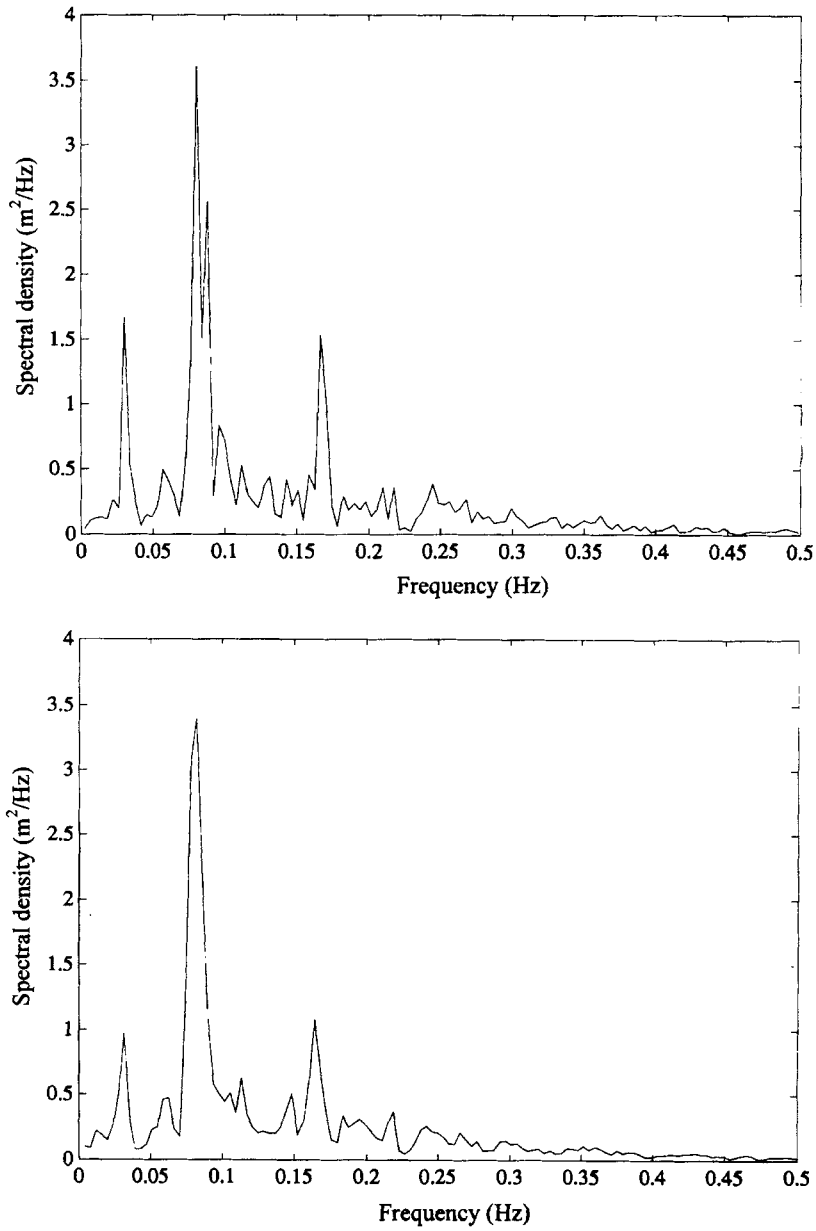

(a) and (b)

Figure 6. Spectra of the water surface elevation record calculated using (a) bin-averaging; (b) segment-averaging with no overlap; and (c) segment-averaging with 50 per cent overlap. For all spectra, $N = 8192$, $f_s = 4$ Hz, $\nu = 16$ (approximately 32 for the 50 per cent overlap), bin width = 0·003906 Hz, and a Hann taper was applied to the time series

factor of m. Hence, deciding on the 'best' spectral density function involves a compromise between the loss of frequency resolution (increasing bin-width) and an increase in the reliability of the spectral estimates (decrease of variance) (Figure 7). This will depend on the type of data and the objectives of the researcher, and is often a matter of trial and error. For the surf zone wave data presented here, it appears that averaging eight bins provides a spectrum which has sufficient resolution and reliability.

When plotting the confidence limits of the spectral density function, it is convenient to plot the ordinate (spectral density) on a logarithmic scale rather than on a linear scale. With a logarithmic ordinate scale the distance between the upper and lower confidence bounds is constant and not dependent upon the value of the spectral density. Hence, the confidence limit may be presented as a single bar (Figure 8). If the height of a peak (or depth of a trough) is greater than the width of the confidence band then the peak (or trough) may be considered to be significant at the chosen significance level. Plotting the auto-spectra on a log-linear scale also helps to highlight energy at the low-frequency end of the spectrum (Figure 8).

Steps in calculating the auto-spectrum

An overview of the recommended steps for estimating the auto-spectral density function is presented below.

1. *Plot the time series* (Figure 1). An important step that should not be overlooked is to plot the time series prior to undertaking spectral analysis. Plotting the time series enables a visual identification of any trend or long-period oscillation in the mean or variance of the series. It is also possible to easily recognize glitches or other outliers in the data that are not consistent with the rest of the time series.
2. *Plot the probability density function* (Figure 2). The probability density function should be plotted and visually compared to a Gaussian distribution. The determination of the confidence limits from the chi-squared distribution assumes that the time series has a Gaussian probability density function.
3. *Detrend.* To satisfy the assumption of stationarity it is necessary to remove any long-term trend from the time series. The resulting time series will have a mean of zero and detrending will ensure that the value of the first Fourier coefficient does not dominate the periodogram.
4. *Apply taper* (Figure 4; Equation 13). An appropriate taper is applied to the detrended time series so that leakage of spectral density from large peaks to adjacent frequency bins is minimized.

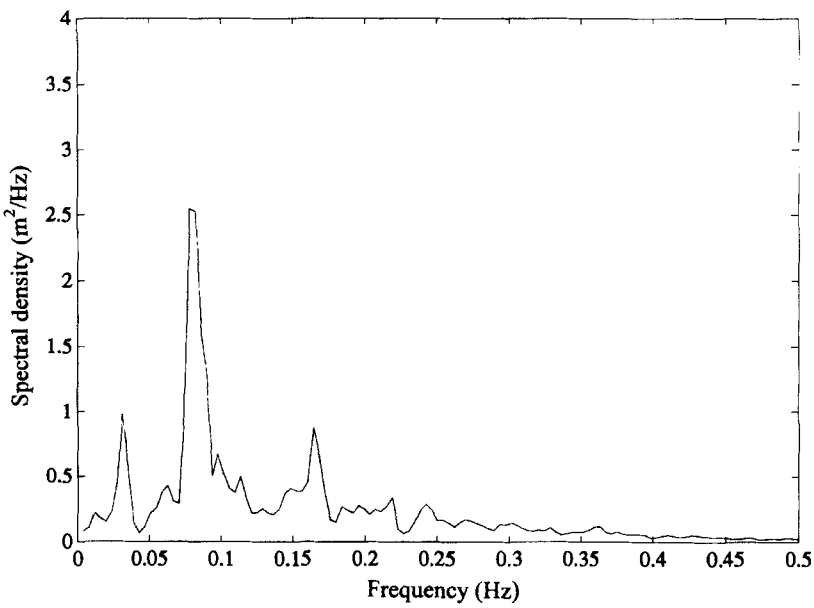

(c)

5. *Calculate discrete Fourier transform (DFT)* (Equation 4). Determine the Fourier coefficients from the detrended and tapered time series using the discrete Fourier transform.
6. *Calculate the one-sided periodogram* (Figure 3; Equation 10).
7. *Correct for tapering* (Equation 14). A correction factor must be applied to each spectral estimate in the periodogram to satisfy Parseval's theorem (Equation 11).
8. *Determine spectral density function* (Figure 6). The spectral density function is determined by combining periodogram estimates using either the bin-averaging or segment-averaging methods. The spectral

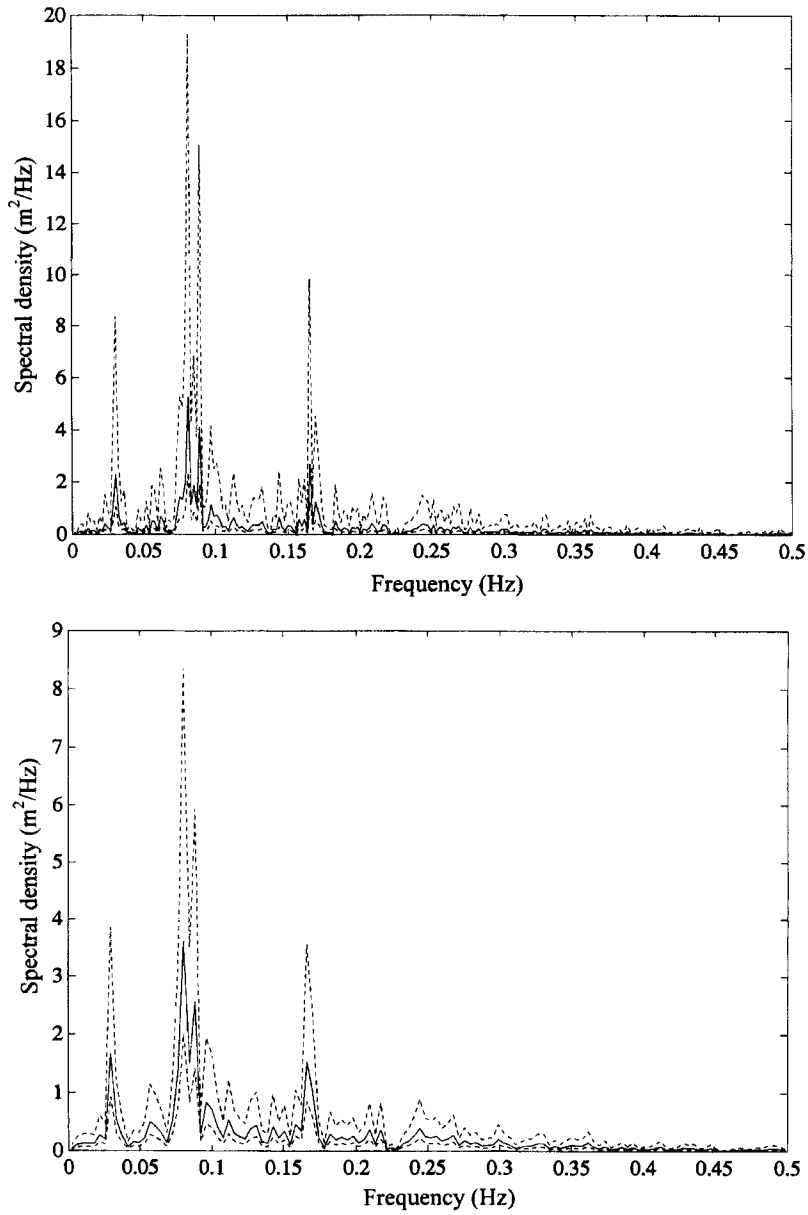

(a) and (b)

Figure 7. Spectra of the water surface elevation record calculated using the bin-averaging method with (a) $m = 4$ ($\nu = 8$, bin width = 0·001953); (b) $m = 8$ ($\nu = 16$, bin width = 0·003906); and (c) $m = 16$ ($\nu = 32$, bin width = 0·007813). For all spectra a Hann taper was applied and $N = 8192$ and $f_s = 4$ Hz. The confidence limits were calculated using a significance level of 0·05

density function is more reliable than the periodogram; however, this is offset by a loss of frequency resolution.

9. *Determine confidence limits* (Figure 8; Equation 15). Confidence limits may be constructed around the auto-spectrum using the degrees of freedom and the chi-squared distribution. This is only appropriate if the probability density function of the time series is approximately Gaussian.

APPLICATIONS AND INTERPRETATION

Two examples have been chosen to highlight the application of spectral techniques to natural time series. These examples are linked and relate to the role of the summer sea breeze in coastal processes along the coastline of Western Australia. The first example employs the auto-spectrum to examine the coastal wind climate during summer and winter and the second example presents an investigation of the nearshore wave climate under the influence of typical sea breeze winds.

Coastal wind climate of Perth, Western Australia

Wind speed and directions were measured hourly on the coast at Ocean Reef, Perth (Western Australia) during 1993 using a standard meteorological station anemometer. The wind speed and direction information was combined to determine two vectors describing the north–south (alongshore) and east–west (cross-shore) wind speed components in units of metres per second. Each component consisted of a total of 8760 points (365 days × 24 hours). An auto-spectral analysis was conducted on both the summer (January–March) and winter (July–September) winds of the north–south component to examine seasonal differences in the wind climate. The auto-spectra were calculated using 2048 points, a Hann taper and bin-averaging using eight adjacent bins (degrees of freedom = 16; bin-width = 0·0938 fractions of an hour). The resulting spectra are presented together in Figure 9 to facilitate comparison between the seasons.

There is a general pattern of decreasing energy with increasing frequency which is typical of natural systems. The winter winds generally had a higher spectral energy than the summer winds across all the frequency bins; this difference is greatest across the lower frequency band (Figure 9). This pattern points to the importance of high energy storm systems that are typically observed along this coast during winter, which result in long periods of relatively high wind velocities prevailing during this season. The summer

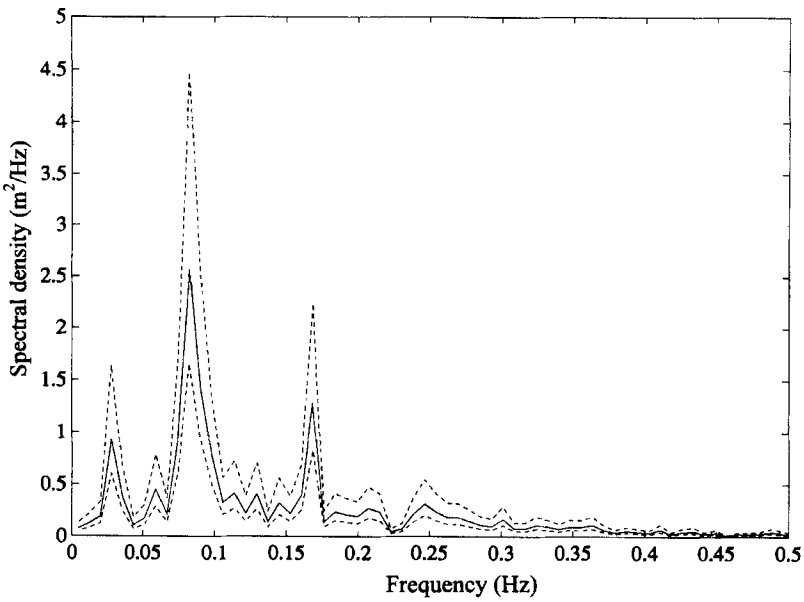

(c)

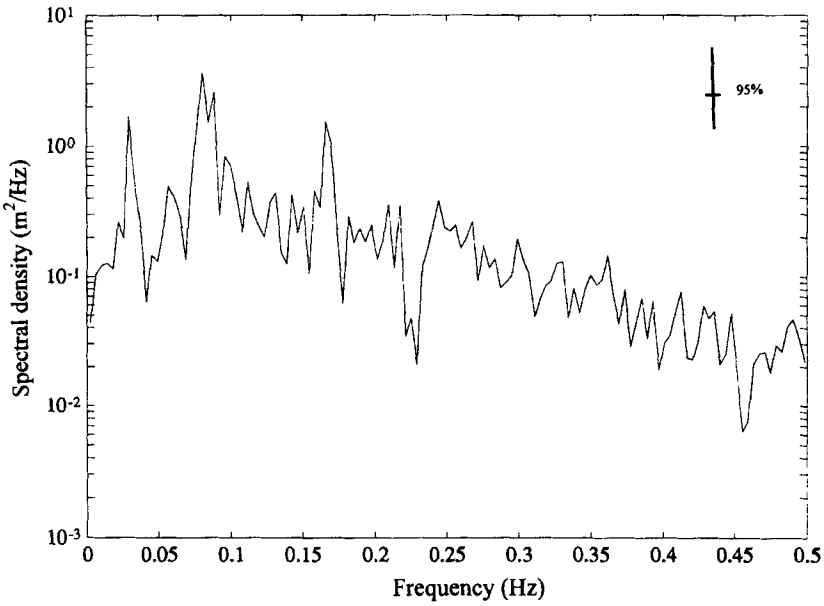

Figure 8. Log spectra of the water surface elevation record calculated using a Hann taper and the bin-averaging method ($N = 8192$, $f_s = 4$ Hz, $\nu = 16$, bin width = 0·003906 Hz). The 95 per cent confidence limits are indicated by the scale bar and were calculated using a significance level of 0·05

spectrum is dominated by a significant peak with a period of 24 hours and testifies to the importance of the diurnal sea breeze system (Figure 9). The sea breeze is particularly significant along this coast during summer and operates as a strong southerly (alongshore) wind that blows during the afternoon on *c.* 60 per cent of summer days with a modal speed in excess of $8{\cdot}3\,m\,s^{-1}$ (Hounam, 1945). During the evening and morning the sea breeze is typically replaced by an offshore easterly breeze. A minor peak at 12 hours is apparent in the summer spectra and appears to represent the first-order harmonic of the 24 hour sea breeze cycle (Figure 9). This harmonic is required to describe the highly asymmetric (non-sinusoidal) nature of the sea/land breeze

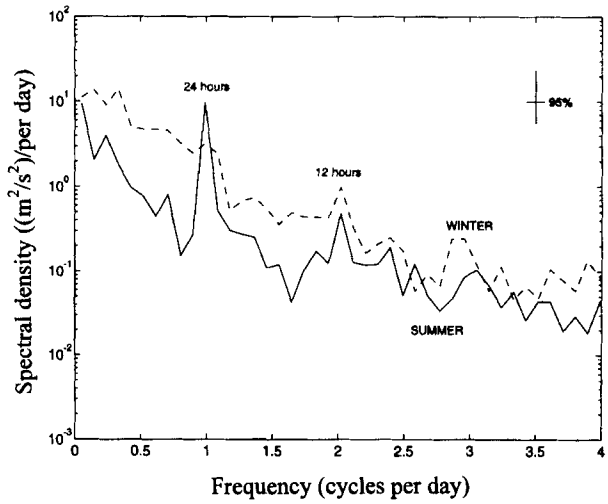

Figure 9. Log spectra of alongshore wind velocity observed at Ocean Reef, Perth (Western Australia) during 1993. The spectra was calculated using a Hann taper and the bin-averaging method ($N = 2048$, $f_s = 1$ per hour, $\nu = 16$, bin width = 0·0938 fractions of an hour). The 95 per cent confidence limits are indicated by the scale bar and were calculated using a significance level of 0·05. Winter winds generally had more energy than the summer winds across all frequencies. The summer spectra is dominated by a peak at 24 hours

cycle (cf. Craddock, 1956; Robert and Richards, 1988). Hence, the 12 hour peak does not appear to have a substantial physical interpretation and is simply an artifact of the Fourier transform which requires a certain number of components to represent the asymmetrical shape of the sea breeze winds.

Nearshore waves under the influence of the sea breeze

To investigate the influence of the sea breeze winds on the nearshore dynamics and morphology, a field experiment was conducted during 3–9 March 1995 at City Beach (Masselink and Pattiaratchi, submitted; Masselink *et al.*, submitted). Data were obtained from a bi-directional acoustic current meter located just beyond the surf zone in an average water depth of 1·5 m. The current velocity was measured in units of metres per second with a sampling frequency of 2 Hz throughout the experiment.

During the period of the field experiment, three distinct sea breeze cycles were observed, between 6 and 9 March 1995. The cross-shore current record was employed to calculate a suite of auto-spectra to cover this three-day period. For the purposes of this analysis the current record was divided into time series segments of 2048 points (nominally 17 minutes). Prior to calculating the auto-spectrum, each time series segment was detrended and Hann-tapered. The variability of the resulting spectral estimates was reduced by averaging 16 adjacent frequency bins resulting in 32 degrees of freedom and a bin-width of 0·0156 Hz. A total of 84 auto-spectra were thus calculated and combined in a three-dimensional time–frequency plot to illustrate the change in spectral signature over the sea breeze cycle observed on 7–8 March 1995 (Figure 10). The background swell waves can be seen in the time–frequency plot as a linear ridge of energy with a frequency which remains between 0·07 Hz (14·3 s) and 0·1 Hz (10 s) throughout the sea breeze cycle (Figure 10). The onset of the sea breeze (14:00 hrs on 7 March 1995) resulted in the emergence of observable wind-wave energy at the high-frequency end of the spectra with peak periods of 2·5 s (Figure 10). As the sea breeze continued to blow throughout the afternoon, the period and energy of the wind waves progressively increased such that at the end of the sea breeze (21:00 hrs on 7 March 1995) the peak period of the wind waves was 4 s. After the sea

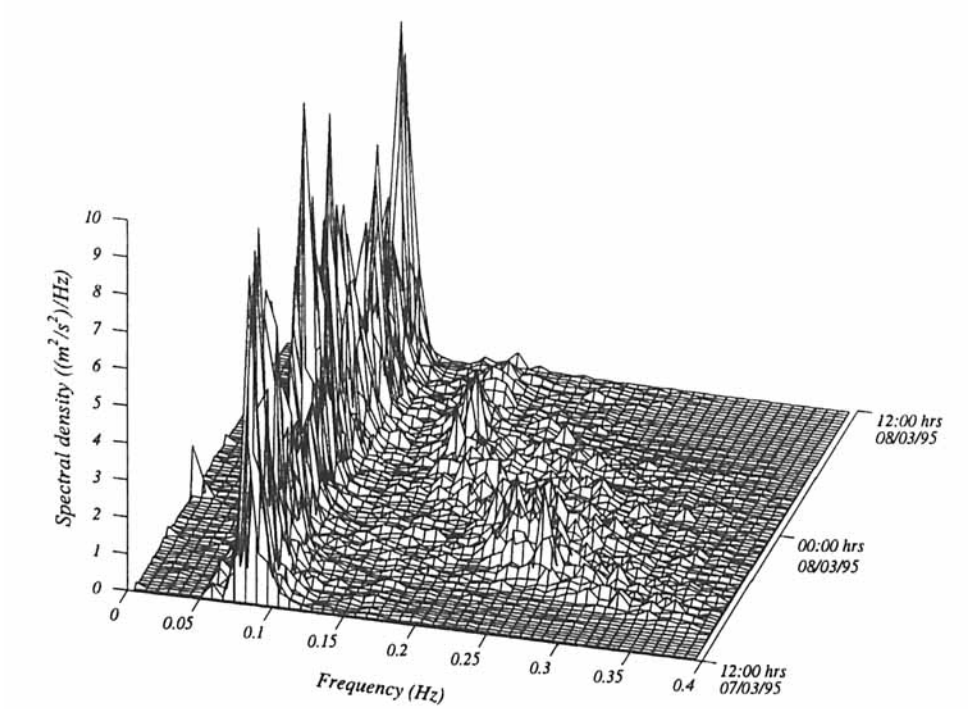

Figure 10. Time–frequency plot of cross-shore currents observed on 7–8 March 1995 at City Beach. Each auto-spectrum was calculated using a Hann taper and the bin-averaging method ($N = 2048$, $f_s = 2$ Hz, $\nu = 32$, bin width = 0·0156 Hz). A ridge of swell wave energy (between 0·07 and 0·1 Hz) is apparent throughout this period and the development of the sea breeze waves can be seen across the high-frequency end of the spectra

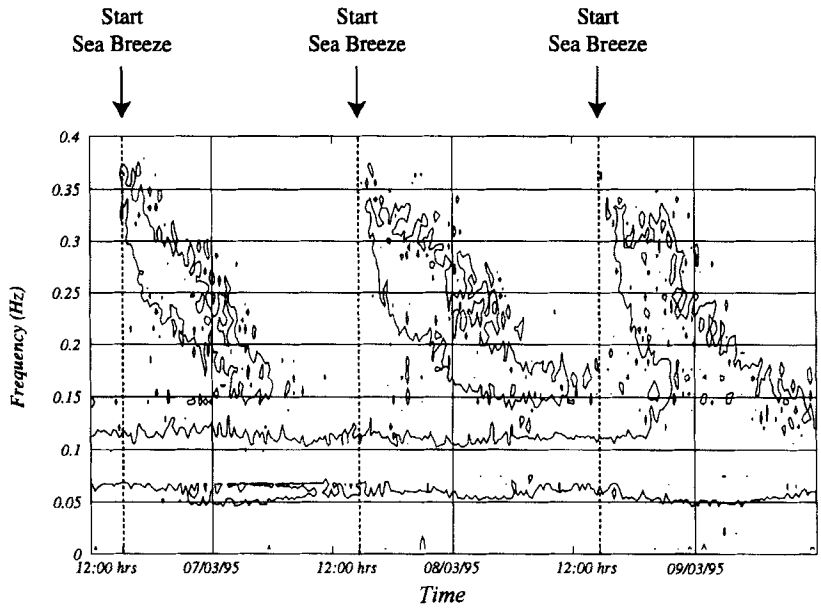

Figure 11. Contour plot of the 0·25 ($m^2 s^{-2}$) Hz^{-1} spectral energy level for the cross-shore current spectra of City Beach observed between 6 and 9 March 1995. Throughout this period the narrow swell band remained centred at a frequency of *c.* 0·085 Hz and the wind wave energy associated with the development of the sea breeze can be seen across the higher frequencies

breeze had subsided, the energy of the wind waves gradually decreased and the frequency of these waves continued to decrease, almost merging with the 'background' swell energy (Figure 10).

A contour diagram of the cross-shore current spectra collected over the three consecutive sea breeze cycles (6–9 March) illustrates more clearly the temporal variation in the frequency components (Figure 11). The contours presented on Figure 11 represent a spectral energy level of 0·25 ($m^2 s^{-2}$) Hz^{-1}. During all three sea breeze cycles the narrow banded swell peak remains centred at a frequency of *c.* 0·085 Hz (11·8 s). The wind wave energy begins to appear immediately after the onset of the sea breeze and is still apparent on the morning of the following day; up to 10 hours after the cessation of the sea breeze (Figure 11). The perseverance of wind wave energy long after the sea breeze has ceased indicates that these waves were generated across a relatively large fetch. However, the offshore limit of the sea breeze is generally considered to be in the order of 50–100 km. On the basis of fetch calculations it appears that these wind waves observed at City Beach were generated at a distance of approximately 300–400 km southeast of the study area by the predominantly longshore component of the sea breeze winds. Hence, the local sea breeze may have regional implications for coastal processes in areas where the sea breeze has a large longshore component.

CONCLUSIONS

This paper outlines the theory involved in Fourier-based spectral techniques and discusses the application and interpretation of these techniques in the calculation of auto-spectra using data sets obtained from natural systems. However, the techniques and methods of spectral analysis outlined in this paper are applicable to any ordered sequence of observation that has been obtained with a uniform sampling interval. It is not the intent of this paper to be a recipe for spectral analysis, but more a didactic framework to enhance the understanding (and hence application) of spectral techniques.

Selecting the 'proper' taper and deciding on the 'best' method to improve the reliability of the spectral estimates depends on the nature of the data series and is often a matter of trial and error. However, it should be noted that a comparison of spectra of different time series is only meaningful if the spectra are calculated under the same conditions. Therefore, when using spectral techniques to analyse multiple time series, the same data length, sampling frequency, taper, spectral estimate averaging method and degrees of freedom

should be employed throughout the analysis. Also, a spectrum which 'looks good', in the sense that it has clearly defined peaks, does not necessarily mean it is the 'right' spectrum. It should always be borne in mind that, like any statistical technique, spectral analysis is a tool, and relationships indicated by the spectral analysis are not necessarily causative.

ACKNOWLEDGEMENTS

The Geography Department of The University of Sydney supported the Nine Mile Beach field campaign. Field assistance for this project was provided by Rob Brander, Adam Cranfield, David Mitchell and Ian Turner. The Ocean Reef wind data were kindly provided by Dr Chari Pattiaratchi. Comments on the manuscript were provided by Dr Saman Abeysekera (Australian Telecommunications Research Institute).

The spectral analysis presented in this paper was completed using a series of fully annotated MATLAB functions written by the authors. These functions are provided freely and are available via e-mail by request to the principal author (bruce@gis.uwa.edu.au).

REFERENCES

Anderson, M. G. and Richards, K. S. 1979. 'Statistical modelling of channel form and process', in Wrigley, N. (Ed.), *Statistical Applications in the Spatial Sciences*, Pion. London, 205–228.

Båth, M. 1974. *Spectral Analysis in Geophysics*, Developments in Solid Earth Geophysics, **7**, Elsevier, Amsterdam, 563 pp.

Beauchamp, K. G. 1984. *Applications of Walsh and Related Functions, with an Introduction to Sequence Theory*, Academic Press, London, 308 pp.

Beauchamp, K. G. and Yuen, C. K. 1979. *Digital Methods for Signal Analysis*, Allen & Unwin, London, 316 pp.

Bendat, J. S. and Piersol, A. G. 1986. *Random Data: Analysis and Measurement Procedures*, 2nd edn, Wiley, Chichester 566 pp.

Bingham, C., Godfrey, M. D. and Tukey, J. W. 1967. 'Modern techniques of power spectrum estimation', *IEEE Transactions of Audio and Electroacoustics*, **AU15**, 56–66.

Blackman, R. B. and Tukey, J. W. 1958. *The Measurement of Power Spectra from the Point of View of Communications Engineering*, Dover Publications, New York, 190 pp.

Carter, R. W. G. 1988. *Coastal Environments: An Introduction to the Physical, Ecological and Cultural Systems of Coastlines*, Academic Press, London, 617 pp.

Chatfield, C. 1985. *The Analysis of Time Series: An Introduction*, 3rd edn, Chapman and Hall, London, 286 pp.

Cooley, J. W. and Tukey, J. W. 1965. 'An algorithm for the machine calculation of complex Fourier series', *Mathematics of Computation*, **19**, 297–301.

Craddock, J. M. 1956. 'The representation of the annual temperature variation over central and northern Europe by a two-term harmonic form', *Quarterly Journal of the Royal Meteorological Society*, **82**, 275–288.

Davis, J. C. 1986. *Statistics and Data Analysis in Geology*, John Wiley, New York, 646 pp.

Ferguson, R. I. 1975. 'Meander irregularity and wavelength estimation', *Journal of Hydrology*, **26**, 315–333.

Ferguson, R. I. 1976. 'Disturbed periodic model for river meanders', *Earth Surface Processes*, **1**, 337–347.

Godin, G. 1972. *The Analysis of Tides*, Liverpool University Press, 264 pp.

Guza, R. T. and Thornton, E. B. 1982, 'Swash oscillations on a natural beach', *Journal of Geophysical Research*, **87**, 483–491.

Hardisty, J. 1993, 'Time series analysis using spectral techniques: oscillatory currents', *Earth Surface Processes and Landforms*, **18**, 855–862.

Holman, R. A. and Sallenger, A. H. Jr. 1985. 'Setup and swash on a natural beach', *Journal of Geophysical Research*, **90**, 945–953.

Hounam, C. E. 1945. 'The sea breeze at Perth', *Weather Developments and Research Bulletin*, **3**, 20–55.

IAHR Working Group on Wave Generation and Analysis. 1989. 'List of sea-state parameters', *Journal of Waterway, Port, Coastal, and Ocean Engineering*, **115**, 793–808.

Jenkins, G. M. and Watts, D. G. 1968. *Spectral Analysis and its Applications*, Holden-Day, San Francisco, 525 pp.

Kay, S. M. and Marple, S. L. 1981. 'Spectrum analysis—A modern perspective', *Proceedings of the IEEE*, **69**, 1380–1419.

Kinsman, B. 1984. *Wind Waves: Their Generation and Propagation on the Ocean Surface*, Dover Publications, New York, 676 pp.

Marple, S. L. 1987. *Digital Spectral Analysis with Applications*, Prentice-Hall, Englewood Cliffs, New Jersey, 492 pp.

Maseslink, G. 1995. 'Group bound long waves as a source of infragravity energy in the surf zone', *Continental Shelf Research*, **15**, 1525–1547.

Masselink, G. and Hegge, B. J. 1996. 'Morphodynamics of mactotidal beaches: Examples from central Queensland, Australia', *Marine Geology*, **129**, 1–29.

Masselink, G. and Pattiaratchi, C. B. (submitted). 'Morphodynamic impact of sea breeze activity on a beach with beach cusp morphology', *Journal of Coastal Research*.

Masselink, G., Hegge, B. J. and Pattiaratchi, C. B. (submitted). 'Beach cusp morphodynamics', *Earth Surface Processes and Landforms*.

MATLAB, 1990. *386-MATLAB for 80386-based MS-DOS Personal Computers: User's Guide*, The MathWorks Inc.

Mulla, D. J. 1988. 'Using geostatistics and spectral analysis to study spatial patterns in the topography of southeastern Washington State, U.S.A.', *Earth Surface Processes and Landforms*, **13**, 389–405.

Press, W. H., Flannery, B. P., Teukolsky, S. A. and Vetterling, W. T. 1989. *Numerical Recipes (Fortran Version)*, Cambridge University Press, 702 pp.

Rayner, J. N. 1971. *An Introduction to Spectral Analysis*, Pion, London, 174 pp.
Richards, K. S. 1976. 'The morphology of riffle–pool sequences', *Earth Surface Processes*, **1**, 71–88.
Robert, A. and Richards, K. S. 1988. 'On the modelling of sand bedforms using the semivariogram', *Earth Surface Processes and Landforms*, **13**, 459–473.
Speight, J. G. 1965. 'Meander spectra of the Angabunga River', *Journal of Hydrology*, **3**, 1–15.
Thakur, T. R. and Scheidegger, A. E. 1970. 'Chain model of river meanders', *Journal of Hydrology*, **12**, 25–47.
Welch, P. D. 1967. 'The use of fast-Fourier transform for the estimation of power spectra: A short method based on time averaging over short, modified periodograms', *IEEE Transactions of the Audio and Electroacoustics*, **AU15**, 70–73.
Young, G. S. and Pielke, R. A. 1983. 'Application of terrain height variance spectra to mesoscale modelling', *Journal of Atmospheric Sciences*, **40**, 2555–2560.
Young, G. S., Pielke, R. A. and Kessler, R. C. 1984. 'A comparison of the terrain height variance spectra of the Front Range with that of a hypothetical mountain', *Journal of the Atmospheric Sciences*, **41**, 1240–1250.